sciendo

Polish Journal of Chemical Technology, 26, 1, 80—87, 10.2478/pjct-2024-0008

Synthesis, structural, thermal, and morphological characterization of Ru(III) complex with gatifloxacin and its utility to obtain RuO_2 nanostructures

Khaled Althubeiti

Department of Chemistry, College of Science, Taif University, P.O. Box 11099, Taif 21944, Saudi Arabia
Corresponding author: e-mail: k.althubeiti@tu.edu.sa

In this work, the reaction between the drug gatifloxacin (as a ligand) with Ru(III) ions was investigated and the resulting complex was structurally and morphologically characterized. The structural properties of the complex were assessed using elemental analyses, molar conductance, thermogravimetry, UV-Vis, and IR spectroscopies, where the morphological characteristics were evaluated using SEM-EDX and XRD methods. The analyses suggested that two ligand molecules were coordinated to the Ru(III) ion via the nitrogen atoms of piperazine rings. The complex was formulated as $[Ru(L)_2(Cl)_2]Cl$, where the Ru(III) ion has a six-coordinate mode, and the coordination sphere is complemented by chlorine atoms. The interaction of the ligand with the Ru(III) ions leads to the product having an organized smooth plate-like structure with a main diameter of 39.42 nm. The RuO_2 oxide in the nanoscale range was generated by the thermal decomposition of the $[Ru(L)_2(Cl)_2]Cl$ complex at 600 °C for 3 hours. SEM micrographs indicated that the RuO_2 material possesses uniform and organized microstructures with many internal cavities enabling it to be used as a catalyst for the heterogeneous degradation of dyes and organic pollutants.

Keywords: Gatifloxacin; Ru(III) ion; Spectroscopy; Morphology; RuO_2 oxide.

INTRODUCTION

Metal complexes are an important class of compounds due to their wide applications ranging from catalysis and material sciences to biology and medicine. Several metal complexes are potentially biologically active and useful as antibacterial, antifungal, and anticancer agents[1–5]. Interactions of quinolones drugs with metal ions have attracted great attention due to their interesting biological and pharmaceutical applications. Numerous research indicated that the interaction between quinolone drugs and metal ions improves their pharmaceutical profiles and more potent biological activity[6–8].

Gatifloxacin, or 1-cyclopropyl-6-fluoro-1,4-dihydro-8-methoxy-7-(3-methyl-1-piperazinyl)-4-oxo-3-quinoline carboxylic acid, is a third-generation fluoroquinolone antibiotic. Its structure is shown in Figure 1. The drug gatifloxacin has a broad spectrum of antimicrobial activities against Gram-negative and Gram-positive bacteria. This drug also possesses anti-inflammatory and antifungal activities[9]. Gatifloxacin molecule can be complexed with metal ions as a uni-dentate ligand using the terminal

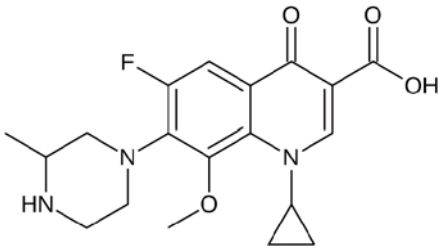

Figure 1. Chemical structure of gatifloxacin

piperazine nitrogen atom, or as a bi-dentate ligand using the carbonyl and carboxyl groups of quinolone ring or the nitrogen atoms of piperazine ring. The interactions of gatifloxacin with several metal ions, like Pd(II), Zn(II), Cr(III), Ni(II), Cd(II), Pt(II), Fe(III), and Co(II), have been investigated and reported in the literature[10–15]. Table 1 lists several examples of gatifloxacin metal complexes.

The purpose of this study was to investigate the metal complex of gatifloxacin (L) with Ru(III) ions and the metal oxide (RuO_2) generated from the thermal decomposition of the metal complex at 600 °C. The resultant

Table 1. Examples of gatifloxacin metal complexes (L: gatifloxacin ligand)

Molar ratio (M:L)	Complexes	Biological Activities	References
1:1	$[X]^+$*fac*-$[RhCl_3(H_2O)(L)]^-$ X: Na or $[H(DMSO)_2]$	antimicrobial activity	[8]
1:1	$[PdCl_2(L)]$	–	[9]
1:2	$[Pt(L)_2]$	Antimicrobial activity DNA cleavage ability DNA binding	[10]
1:2	$[Ni(L)_2(H_2O)_2]\cdot 4H_2O$ $[Co(L)_2(H_2O)_2]\cdot 4H_2O$ $[Zn(L)_2(H_2O)_2]\cdot 4H_2O$	Antimicrobial activity	[11]
1:2	$[Cu(L)_2(H_2O)_2]\cdot H_2O$ $[Zn(L)_2(H_2O)_2]\cdot 2H_2O$ $[Fe(L)_2Cl(H_2O)_2]Cl\cdot 2H_2O$ $[Mn(L)_2(H_2O)_2]\cdot 6H_2O$ $[Mg(L)_2(H_2O)_2]Cl_2\cdot H_2O$ $[Cr(L)_2Cl(H_2O)_2]Cl\cdot 2H_2O$	Antiiinflamatory Antifungal activity Antimicrobial activity	[12]
1:3	$[Bi(L)_3(H_2O)_2]$	Helicobacter pylori Antimicrobial activity	[13]

$[Ru(L)_2(Cl)_2]Cl$ complex was characterized by CHN elemental analysis, magnetic susceptibility and molar conductance measurements, and spectroscopic data (UV-Vis, and IR). The $[Ru(L)_2(Cl)_2]Cl$ complex was thermally decomposed at 600 °C for 3 hours to obtain the nanostructured RuO_2 oxide, and the resultant oxide was characterized by scanning electron microscopy (SEM) and X-ray diffraction (XRD) methods.

EXPERIMENTS

Chemicals and instrumentation

The chemicals used in this work were analytical grade chemicals and included gatifloxacin ($C_{19}H_{22}FN_3O_4$; 375.4 g/mol) obtained from the Fluka Company (Seelze, Germany), and ruthenium(III) chloride hydrate ($RuCl_3$ xH_2O; 207.43 g/mol) obtained from the Sigma-Aldrich Company (St Louis, MO, USA). Analytical measurements were conducted using a Jenway 4010 conductivity meter for determining the conductivity of complex dissolved in DMSO at a concentration of 1×10^{-3} M, and a Perkin–Elmer 2400 series CHN elemental analyzer for collecting the carbon, hydrogen, and nitrogen contents. Ruthenium and water contents were determined gravimetrically. Thermal measurements were acquired using a Shimadzu TG/DTG-50H thermal analyzer in a nitrogen atmosphere for obtaining the TGA and DTA thermograms over the temperature range of 25–1000 °C. The spectral measurements were acquired at room temperature using an X'Pert Philips X-ray diffractometer for recording XRD spectra with 2θ between 20° and 100°, a Perkin-Elmer Lambda 25 UV/Vis spectrophotometer for scanning UV–Vis spectra (DMSO solvent) from 200 to 800 nm, and a Shimadzu FT-IR spectrophotometer for scanning infrared (IR) spectra from 4000 to 400 cm^{-1}. A Quanta FEI 250 scanning electron microscope (SEM) (20 kV accelerating voltage) integrated with an EDAX detector was used to visualize the structural morphologies and record the EDX profile.

Preparations

The $[Ru(L)_2(Cl)_2]Cl$ complex was prepared from the reaction of gatifloxacin as a ligand (L) with Ru(III) ions with a 1:2 metal to the ligand. An aqueous solution (25 mL) containing 2 mmol of $RuCl_3$ xH_2O was mixed with a methanolic solution (25 mL) containing 4 mmol of the ligand. The pH of the mixture was adjusted to 7–8 using ammonium solution (5%), then the mixture was refluxed for 6 hours at 80 °C. After cooling, the resulting dark-brown precipitate was filtered off, thoroughly washed, and oven-dried at 70 °C. The purified complex was next characterized by elemental, thermal, and spectral analyses. The $[Ru(L)_2(Cl)_2]Cl$ complex was calcined at 600 °C for 3 hours in an electric furnace to generate RuO_2 metal oxide.

RESULTS AND DISCUSSION

Characterization the metal complex

Elemental and Molar conductivity measurements

To prepare the metal complex, the ligand was dissolved in methanol solvent, where the Ru(III) ion was dissolved in Milli-Q purified water. Refluxing the Ru-(III)-ligand mixture (1:2 metal to ligand ratio) generated a dark-brown solid material which was formulated as $[Ru(L)_2(Cl)_2]Cl$. The complex was insoluble in water and most organic solvents, except *N*,*N*-dimethylformamide-based (DMF), and dimethyl sulfoxide (DMSO) solvents. Carbon, hydrogen, and nitrogen contents in the complex were determined using elemental analysis, where the Ru element was determined gravimetrically. A sample of the solid complex gave the following elemental results in (%) (C 47.35, H 4.84, N 8.52, and Ru 10.76). These elemental results suggest that the complex was formulated as $[Ru(L)_2(Cl)_2]Cl$. The gross formula of the complex is $C_{38}H_{44}F_2N_6O_8RuCl_3$ (958.15 g/mol). The theoretical elemental results in (%) (C 47.59, H 4.59, N 8.77, and Ru 10.54). The molar conductance value of the free ligand was 0.15 μS. After the ligand complexed with Ru(III) ion, the molar conductance increased to 0.68 μS. The molar conductance of the complex suggested that one chloride ion exists outside of the complex's coordination sphere.

UV–Vis spectra

Figure 2 contains the UV-Vis spectra of the free ligand and $[Ru(L)_2(Cl)_2]Cl$ complex. The free ligand molecule showed three absorption bands at 339, 354, and 367 nm in its UV-Vis spectrum. The band that resonated at 339 nm was assigned to the $\pi\rightarrow\pi^*$ transitions for the aromatic rings, whereas the bands that appeared at 354 and 367 nm were attributed to the $n\rightarrow\pi^*$ transitions for the ketonic and carboxylic groups and piperazine ring. After the ligand complexed with Ru(III) ion, these absorption bands were shifted to a lower wavelength and appeared at 339, 352, and 361 nm. The shifting to a lower wavelength could be due to the intra-molecular interaction. The band at 339 nm is due to the $^2T_{2g}\rightarrow{}^4T_{1g}$ transition, whereas the band at 352 nm is due to the $^2T_{2g}\rightarrow{}^2A_{2g}$ transition[16, 17].

IR spectra

Figure 3 contains the IR spectra of the free ligand and $[Ru(L)_2(Cl)_2]Cl$ complex. The free ligand molecule has several different functional groups: N–H, C–N, O–H, C=O, C–O, C=C, and C–F. These groups generated several stretching and bending vibrations, namely $\nu(N-H)_{piperazine}$, $\nu(O-H)$, $\nu_{sym}(C-N)$, $\nu(C=O)_{carboxylic}$, $\nu(C=O)_{ketonic}$, $\nu(C=C)$, $\nu(C-O)$, and $\nu(C-F)$, which appeared at 3397, 3223, 1318, 1721, 1622, 1546, 1207, and 1146 cm^{-1}, respectively. The bands located at 2957 and 2844 cm^{-1} resulted from the $\nu_{asym}(C-H)$ and $\nu_{sym}(C-H)$ vibrations of CH_3, CH_2, and CH moieties. Free ligand molecule has five $-CH_2$ groups. These methylene groups generated absorption bands at 1349, 1268, 730, and 643 cm^{-1} due to the $\delta_{sciss}(CH_2)$, $\delta_{rock}(CH_2)$, $\delta_{wag}(CH_2)$, and $\delta_{twist}(CH_2)$ vibrational modes, respectively[18]. Free ligand molecule also has two $-CH_3$ groups. These methyl groups generated absorption bands at 1438 and 821 cm^{-1} due to the

$\delta_{rock}(CH_3)$, and $\delta_{wag}(CH_3)$ vibrational modes, respectively [18]. The IR spectrum of the complex contained absorption bands at 3380, 3153, (2950 and 2832), 1723, 1620, 1510, 1439, 1320, 1270, 1213, 1139, 1045, 995, 891, 800, 735, and 650 cm^{-1} that originated, respectively, from the bending and stretching vibrations of $\nu(N-H)_{piperazine}$, $\nu(O-H)$, $\nu_{asym}(C-H)$ and $\nu_{sym}(C-H)$, $\nu(C=O)_{carboxylic}$, $\nu(C=O)_{ketonic}$, $\nu(C=C)$, $\delta_{rock}(CH_3)$, $\delta_{sciss}(CH_2)$, $\delta_{rock}(CH_2)$, $\nu_{asym}(C-N)$, $\nu(C-F)$, $\nu_{sym}(C-N)$, $\delta(C-C)$, $\delta_{def}(C-H)$, $\delta_{wag}(CH_3)$, $\delta_{wag}(CH_2)$, and $\delta_{twist}(CH_2)$, respectively. The complexation of the ligand with Ru(III) ion affects the band resulting from the $\nu(N-H)_{piperazine}$ vibration. The band become broader, and its frequency was shifted to a lower wavenumber. The complexation of the ligand with Ru(III) ion doesn't affect the bands resulting from the $\nu(C=O)_{carboxylic}$ and $\nu(C=O)_{ketonic}$ vibrations. Several bands that were generated from the CH_3 and CH_2 vibrational modes were shifted due to the complexation process. New broadband with medium intensity appeared at 510 cm^{-1} in the IR spectrum of the complex and could be assigned to the $\nu(Ru-N)$ vibration[19]. All these observations suggest that the ligand coordinated with the Ru(III) ion via nitrogen atoms of the piperazine ring.

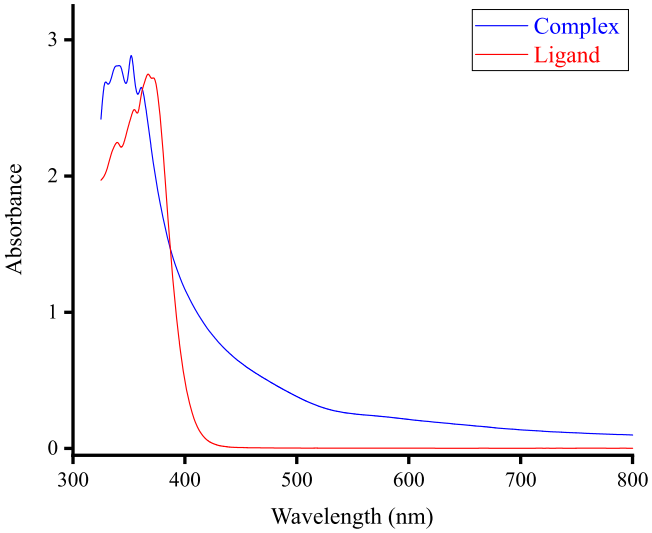

Figure 2. The UV-Vis spectra of the free ligand and $[Ru(L)_2(Cl)_2]Cl$ complex at a concentration of 1×10^{-3} M

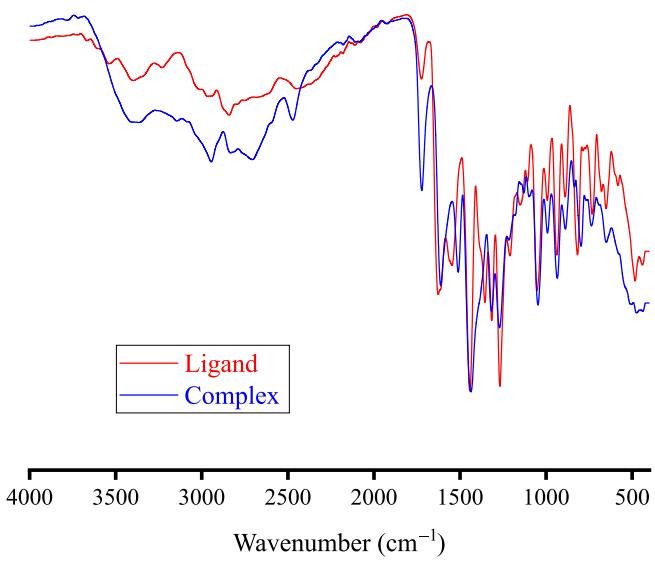

Figure 3. The IR spectra of the free ligand and $[Ru(L)_2(Cl)_2]Cl$ complex

XRD spectra

Figure 4 presents the observed XRD patterns of $[Ru(L)_2(Cl)_2]Cl$ complex. The complex displayed one broad peak ranging from $2\theta\sim25^o$ to $\sim60^o$. This broadband contains a strong and sharp line at Bragg's angle 2θ 32.6607°. This XRD profile suggests that the complex mainly possesses an amorphous structure. A group of low-intense lines was also observed in the XRD diffractogram of the complex. These lines are located exactly at 2θ 46.758°, 52.791°, and 58.413°. The intense diffraction line at 32.6607° corresponded to the reflection plane (002) for typical Ru. The low-intensity lines appeared at 46.758° and 52.791° associated with Bragg's reflections (100) and (101), respectively, for typical Ru[20]. The broadening of the most intense diffraction line (32.6607°) was used in calculating the average particle diameters (D) using the Debye–Scherrer's formula[21]: $[D = 0.94\lambda /\beta \cos \theta]$. The calculated D value was 39.42 nm, suggesting that the synthesized $[Ru(L)_2(Cl)_2]Cl$ complex was nanoscale-sized.

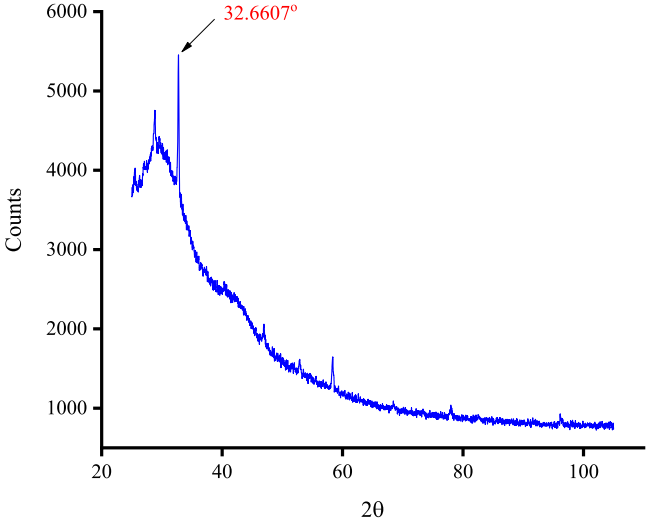

Figure 4. The XRD diffractogram of the $[Ru(L)_2(Cl)_2]Cl$ complex

Thermal measurements

Figure 5 contains the TGA and DTA thermograms of the free ligand and $[Ru(L)_2(Cl)_2]Cl$ complex. The free ligand molecule decomposed in three degradation steps and showed complete degradation without any remaining carbon. The three decomposition steps for the free ligand occurred within the temperature ranges of 220–315, 315–450 and 450–700 °C. The first step was assigned to the removal of a methoxy and a cyclopropyl group and corresponding to weight losses of (cal. = 19.18%, obs. = 18.95%). The second step was assigned to the removal of 1-methyl piperazine and corresponding to weight losses of (cal. = 26.37%, obs. = 26.55%). The weight losses in the last step were (cal. = 54.45%, obs. = 54.30%), corresponding to the release of the 6-fluoro-1,4-dihydro--4-oxo-3-quinoline carboxylic acid organic moiety. The $[Ru(L)_2(Cl)_2]Cl$ complex exhibited a three-stage degradation process, and the decomposition of the complex resulted in Ru as the final degradation product. The three decomposition steps of the complex occurred within the temperature ranges of 70–200, 200–375, and 375–600 °C, corresponding to weight losses of (cal. = 11.10%, obs. = 11.32%), (cal. = 39.18%, obs. = 39.35%), and (cal. =

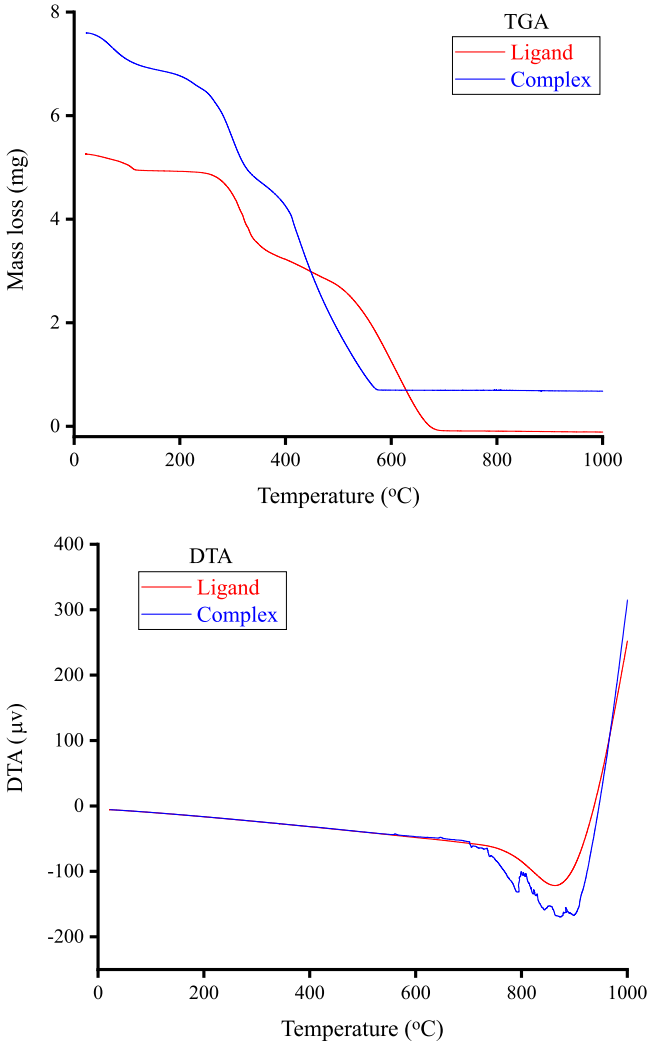

Figure 5. A) The TGA plots of the free ligand and $[Ru(L)_2(Cl)_2]Cl$ complex; B) The DTA plots of the free ligand and $[Ru(L)_2(Cl)_2]Cl$ complex

39.18%, obs. = 93.02%), respectively. The three chlorine atoms in the complex were released in the first step. The release of the first ligand molecule began and finished in the second degradation step, whereas the pyrolysis of the second ligand molecule began and finished in the last degradation step. The final decomposition product of the complex was Ru (cal. = 10.54%, obs. = 10.80%) free of any residual carbons. The DTA thermogram of the complex shows a strong endothermic peak in the 840–900 °C range without any weight loss. This broad peak was assigned to the formation of nanostructured Ru metal with transformation change in the physicochemical properties[17, 22].

SEM-EDX analysis

Microstructure, porous structure of the surface, surface topology, and other outer surface-related information about the material can be collected using a scanning electron microscope (SEM). SEM micrographs of the $[Ru(L)_2(Cl)_2]Cl$ complex were captured at different levels of magnification (i.e., x1000, x2500, x5000, x10000, and x20000) using a Quanta FEI 250 SEM instrument. Figure 6 illustrates the SEM-EDX data of the complex. The SEM micrographs indicated that the particles of the complex have distinct sizes and morphology. The complex had a large and well-smooth plate-like structure. This morphology gives the complex a large surface. The plates have several clear visible cracks, and small granules of different sizes and shapes accumulate on the plate's surface. The EDX spectrum of the complex evidenced the presence of F, Cl, O, C, and Ru elements. The Ru element displayed a strong, intense line at 2.55 keV.

Proposed complex's structure

Spectral, thermal, and elemental results proposed that the ligand acts as a bidentate ligand coordinated to the Ru(III) ion through the nitrogen atoms of piperazine rings. The complex has the general formula $[Ru(L)_2(Cl)_2]Cl$. The Ru(III) ion has a six-coordinate mode, and the coordination sphere is complemented by chlorine atoms (Fig. 7).

Characterization the metal oxide

Spectral properties

The metal oxide (RuO_2) was generated by the direct thermal decomposition of the $[Ru(L)_2(Cl)_2]Cl$ complex. The decomposition was processed in an electric furnace for 3 hours at 600 °C. The nanostructured RuO_2 material was ground into a fine powder with particle sizes of ~5 mm. The IR spectrum of the RuO_2 material is shown in Figure 8. The spectrum was characterized by three IR absorption bands with medium intensity in the region 1700–1200 cm^{-1} and could be assigned to the vibrations of physically adsorbed water (moisture) on the RuO_2 surface. Also, a broad band was observed at around 420 cm^{-1}. The three medium-intensity bands located at 1735, 1360, and 1215 cm^{-1}, and attributed to the vibrations of ν(O–H) of molecular water (ν6), peroxo groups (ν5), and peroxo groups (ν4), respectively. The absorptions at 420 cm^{-1} could be assigned to the (ν1) asymmetric stretching vibration characteristic of RuO_2[23, 24]. The RuO_2 material was scanned by an XRD instrument to confirm its framework structure and phase purity, and the XRD patterns are shown in Figure 9. The XRD profile displayed a narrow sharp and very strong diffraction pattern at a 2θ 44.070°. This diffraction peak suggests that the RuO_2 material is crystalline in nature and has a well-defined and well-organized morphology. The RuO_2 displayed three XRD reflections with a medium intensity that was observed at Bragg's angle 2θ value of 28.105°, 35.082°, and 54.330°. Also, the profile of RuO_2 displayed a group of low-intensity peaks appeared at diffraction angles 2θ of 38.427°, 42.059°, 58.208°, 69.473°, 78.358°, and 84.801°. The XRD reflections located at Bragg's angle 2θ value of 78.358°, 69.473°, 54.330°, 44.070°, 42.059°, and 28.105°, could be assigned to (311), (301), (220), (210), (020), and (110) reflections of crystal RuO_2 phase, respectively. The observed XRD patterns indicated that the RuO_2 material has an orthorhombic structure (JCPDS No: 88−0323). This profile matches well with the profiles previously reported by K.A. Alibrahim *et. al.*, 2019[25] and M.S. Refat *et. al.*, 2021 [26]. The D value of the RuO_2 material was determined from its XRD patterns based on the highest-intensity line at 2θ 44.070°. The calculated D value was 38.5 nm, suggesting that the RuO_2 crystallites are nanoscale.

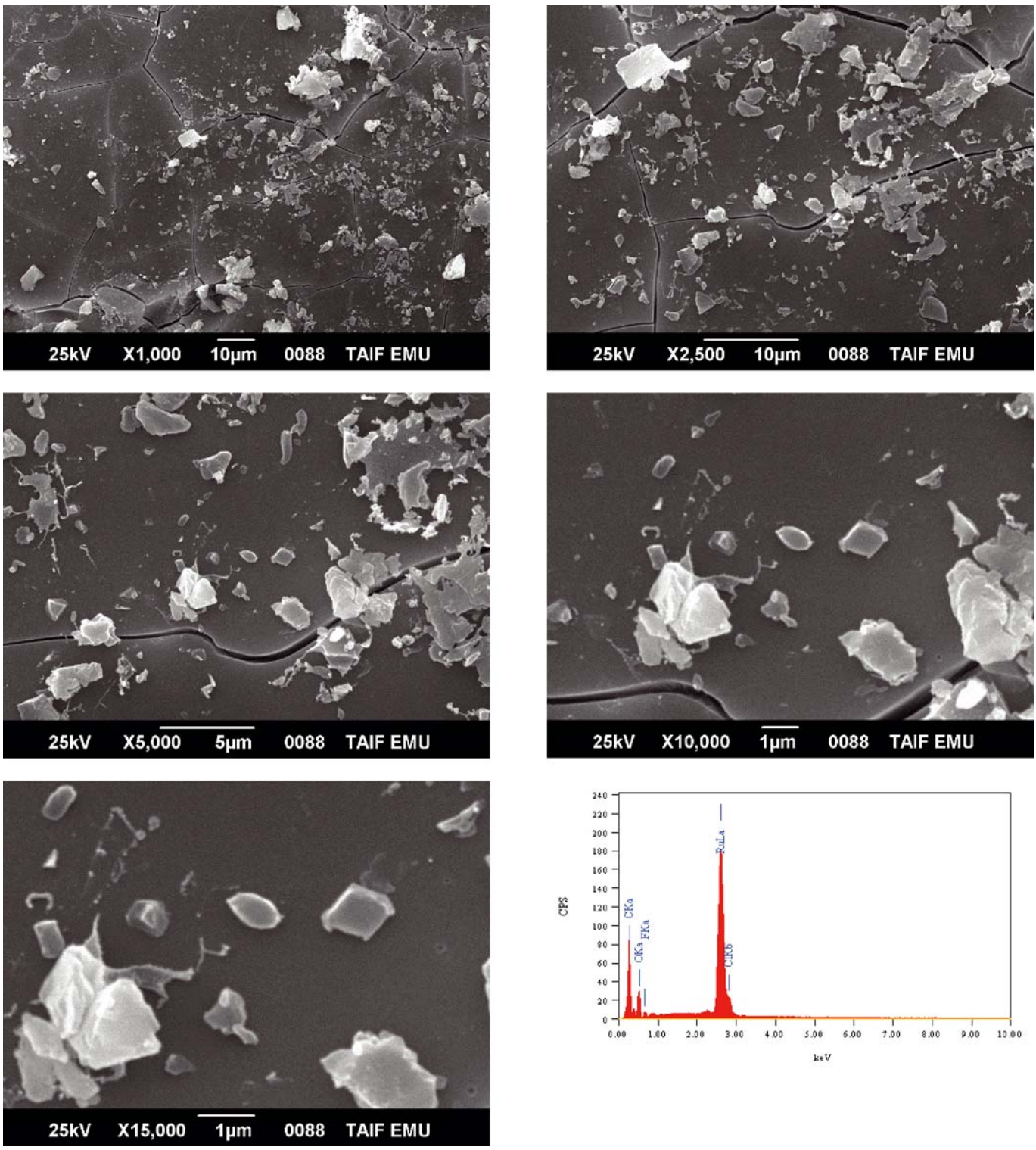

Figure 6. The SEM-EDX data of the $[Ru(L)_2(Cl)_2]Cl$ complex

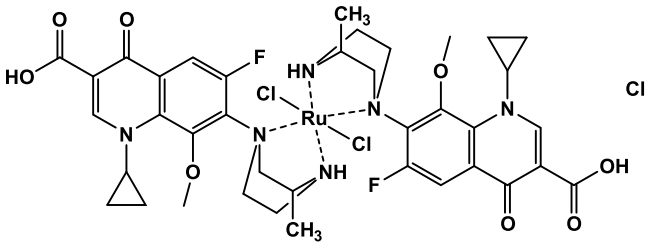

Figure 7. Proposed chemical structure of the synthesized complex; $[Ru(L)_2(Cl)_2]Cl$

Morphological properties

SEM micrographs of the RuO_2 material were captured at different degrees of enlargement (i.e., x1500, x2500, x5000, x10000, and x15000) using a Quanta FEI 250 SEM instrument. The well-focused SEM micrographs presented in Figure 10, indicate that the RuO_2 material has a distinct morphology. The highly magnified (x10000, and x15000) micrographs indicated that the RuO_2 material consists of granules of semi-spherical or oval shapes fused and forming large pieces. The micrographs captured at low magnification (x2500, and x500), indicated that the large pieces were agglomerated and formed long, twisted chains, resembling the walls of a maze. This morphology provides the RuO_2 material with many internal cavities that enable it to absorb other substances inside it. Based on this morphology, the RuO_2 material can be used as a catalyst for the heterogeneous degradation of dyes and organic pollutants. The EDX spectrum (Fig. 10)

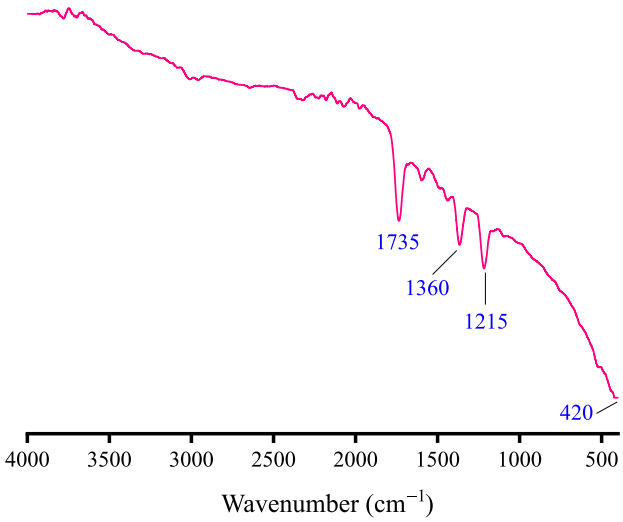

Figure 8. The IR spectrum of the RuO_2 material

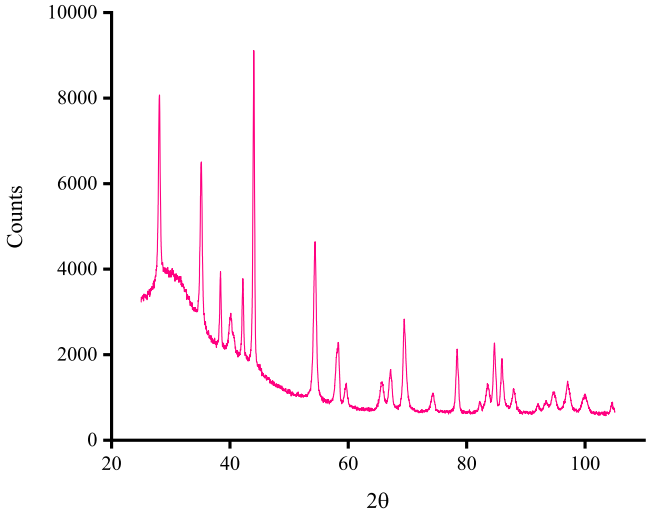

Figure 9. The XRD diffractogram of the RuO_2 material

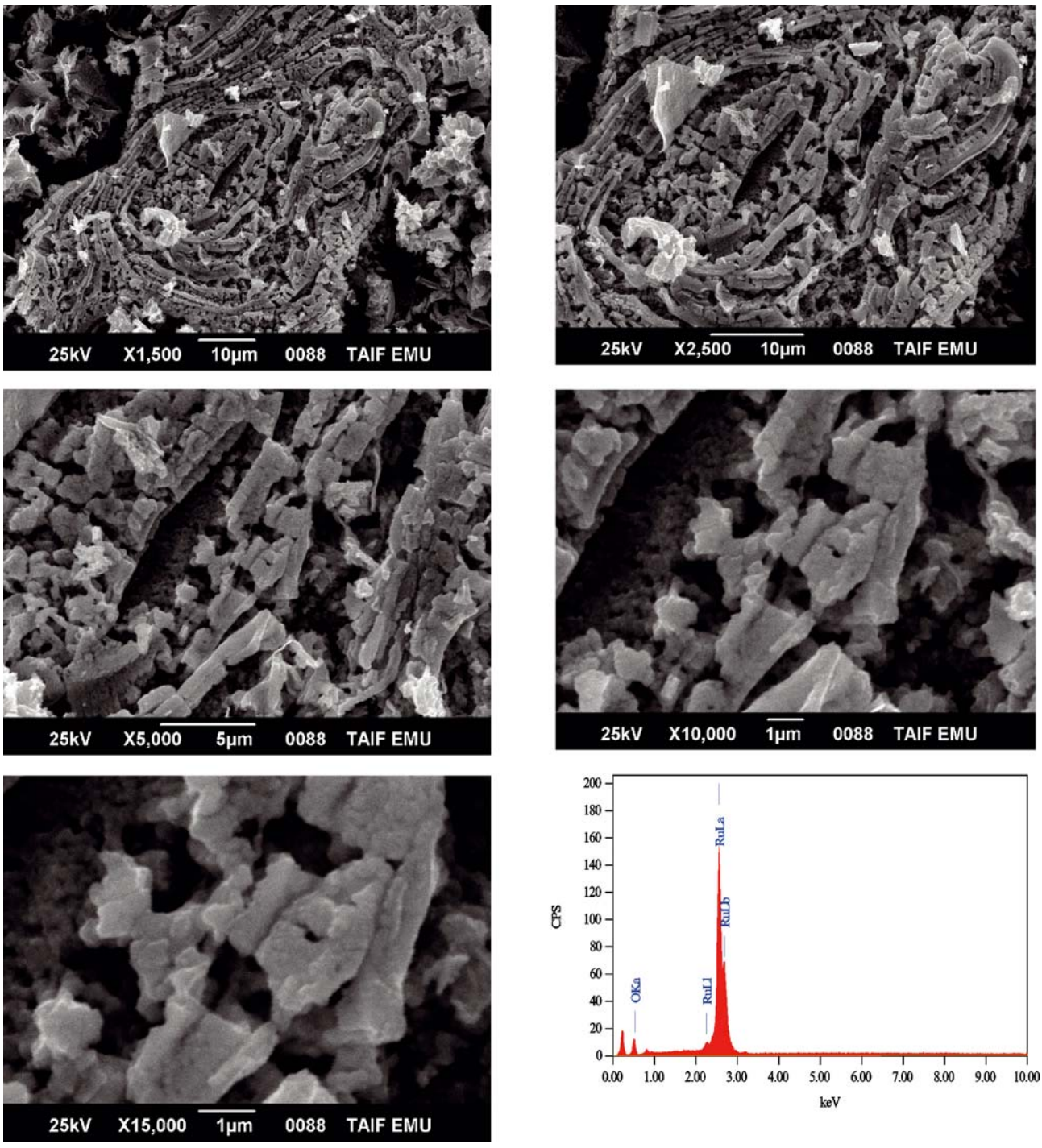

Figure 10. The SEM-EDX data of the of the RuO_2 material

of the RuO_2 material evidenced the presence of oxygen and ruthenium elements without any organic impurities.

CONCLUSIONS

In this study, the antibiotic drug gatifloxacin was complexed with Ru(III) ions at a 1:2 metal-to-ligand ratio. The synthesized complex was structurally characterized by physicochemical and spectroscopic techniques, the results of which supported that the formulae of the complex was $[Ru(L)_2(Cl)_2]Cl$. In the complex, the Ru(III) ions are coordinated with the two nitrogen atoms inside the ligand's piperazine ring. The Ru(III) ion has a six-coordinate mode, and the coordination sphere is complemented by chlorine atoms. The average particle diameters (*D*) of the $[Ru(L)_2(Cl)_2]Cl$ complex was 39.42 nm, and this value indicates that the particle sizes of the complex are within the nanoscale range. The $[Ru(L)_2(Cl)_2]Cl$ complex was used to generate the nanostructured RuO_2 material via direct thermal decomposition in the air. The XRF analysis confirms the orthorhombic structure of RuO_2 with a crystallite size of 38.5 nm. SEM data showed that the RuO_2 material possesses uniform and organized microstructures with many internal cavities enabling it to be used as a catalyst for the heterogeneous degradation of dyes and organic pollutants.

ACKNOWLEDGEMENT

The authors extend their appreciation to Taif University, Saudi Arabia, for supporting this work through Project number (TU-DSPP-2024-59).

LITERATURE CITED

1. Tella, A.C., Obaleye, J.A., Olawale, M.D., Ngororabanga, J.M.V., Ogunlaja, A.S. & Bourne, S.A. (2019). Synthesis, crystal structure, and density functional theory study of a zinc(II) complex containing terpyridine and pyridine-2,6-dicarboxylic acid ligands: Analysis of the interactions with amoxicillin. *C.R. Chimie*. 22(1), 3–12. DOI: 10.1016/j.crci.2018.11.007.

2. Helaly, A.A., El-Bindary, A.A. & Elsayed, S.A. (2023). Synthesis and characterization of Co(II), Ni(II), Cu(II) and Zn(II) chelates: DFT calculations, molecular docking and biological applications. *J. Mol. Liq*., 389, 122831. DOI: 10.1016/j.molliq.2023.122831.

3. Eichhorn, G.L. & Marzilli, L.G. (1994). *Advances in Inorganic Biochemistry Models in Inorganic Chemistry*, PTR Prentice-Hall, Inc, New Jersey, USA.

4. El-Bindary, M.A. & El-Bindary, A.A. (2022). Synthesis, characterization, DNA binding, and biological action of dimedone arylhydrazone chelates. *Appl. Organomet. Chem*., 36(4), e6576. DOI: 10.1002/aoc.6576.

5. Rezk, G.N., El-Gammal, O.A., Alrefaee, S.H., Althagafi, I., El-Bindary, A.A. & El-Bindary, M.A. (2023). Synthesis, structural characterization, antioxidant, cytotoxic activities and docking studies of schiff base Cu(II) complexes. *Heliyon*, 9, e21015. DOI: 10.1016/j.heliyon.2023.e21015.

6. Fricker, S.P. (2007). Metal based drugs: from serendipity to design. *Dalton transactions*, 43, 4903–4917. DOI: 10.1039/B705551J.

7. Jurowska, A., Jurowski, K., Szklarzewicz, J., Buszewski, B., Kalenik, T. & Piekoszewski, W. (2016). Molybdenum Metallopharmaceuticals Candidate Compounds - The "Renaissance" of Molybdenum Metallodrugs?. *Cur. Med. Chem*., 23(29), 3322–3342.

8. Efthimiadou, E.K., Thomadaki, H., Sanakis, Y., Raptopoulou, C.P., Katsaros, N., Scorilas, A., Karaliota, A. & Psomas, G. (2007). Structure and biological properties of the copper(II) complex with the quinolone antibacterial drug N-propyl-norfloxacin and 2,2′-bipyridine. *J. Inorg. Biochem*., 101, 64–73. DOI: 10.1016/j.jinorgbio.2006.07.019.

9. Oliphant, C.M. & Green, G.M. (2002). Quinolones: a comprehensive review. *Am. Fam. Phys*., 65, 455–464.

10. Mehrotra, R., Shukla, S.N., Gaur, P. & Dubey, A. (2012). Identification of pharmacophore in bioactive metal complexes: Synthesis, spectroscopic characterization and application. *Eur. J. Med. Chem*., 50, 149–153. DOI: 10.1016/j.ejmech.2012.01.049.

11. Vieira, L.M.M., de Almeida, M.V., Lourenço, M.C.S., Bezerra, F.A.F.M. & Fontes, A.P.S. (2009). Synthesis and antitubercular activity of palladium and platinum complexes with fluoroquinolones. *Eur. J. Med. Chem*., 44, 4107–4111. DOI: 10.1016/j.ejmech.2009.05.001.

12. Patel, M.N., Gandhi, D.S. & Parmar, P.A. (2012). DNA interaction and in-vitro antibacterial studies of fluoroquinolone based platinum(II) complexes. *Inorg. Chem. Commun*., 15, 248–251. DOI: 10.1016/j.inoche.2011.10.037.

13. Li, Z.-Q., Wu, F.-J., Gong, Y., Hu, C.-W., Zhang, Y.-H. & Gan, M.-Y. (2007). Synthesis, Characterization and Activity against *Staphylococcus* of Metal(II)-Gatifloxacin Complexes. *Chin. J. Chem*., 25, 1809–1814. DOI: 10.1002/cjoc. 200790334.

14. Sultana, N., Naz, A., Arayne, M.S. & Ahmed, M.M. (2010). Synthesis, characterization, antibacterial, antifungal and immunomodulating activities of gatifloxacin–metal complexes. *J. Mol. Struct*., 969, 17–24. DOI: 10.1016/j.molstruc. 2010.01.036.

15. Shaikh, A.R., Giridhar, R., Megraud, F. & Yadav, M.R. (2009). Metalloantibiotics: Synthesis, characterization and antimicrobial evaluation of bismuth-fluoroquinolone complexes against Helicobacter pylori. *Acta Pharm*., 59, 259–271. DOI: 10.2478/v10007-009-0027-6.

16. Althubeiti, K. (2020). In binary solvent: Synthesis and physicochemical studies on the nano-metric palladium(II) oxide associated from complexity of palladium(II) ions with gatifloxacin drug as a bio-precursors, *J. Mol. Struct*., 1205, 127604. DOI: 10.1016/j.molstruc.2019.127604.

17. Naglah, A.M., Al-Omar, M.A., Almehizia, A.A., Obaidullah, A.J., Bhat, M.A., Al-Shakliah, N.S., Belgacem, K., Majrashi, B.M., Refat, M.S. & Adam, A.M.A. (2020). Synthesis, Spectroscopic, and Antimicrobial Study of Binary and Ternary Ruthenium(III) Complexes of Ofloxacin Drug and Amino Acids as Secondary Ligands, *Crystals*, 10(3), 225. DOI: 10.3390/cryst10030225.

18. Sathyanarayana, D.N. (2004). *Vibrational Spectroscopy-Theory and Applications*, second ed., New Age International (P) Limited Publishers, New Delhi, India.

19. Nakamoto, K. (1970). *Infrared Spectra of Inorganic and Coordination Compounds*, Wiley Interscience, John Wiley & Sons, 2nd edition, New York, NY, USA.

20. Singh, J.P., Karabacak, T., Morrow, P., Pimanpang, S., Lu, T.-M. & Wang, G.-C. (2007). Preferred Orientation in Ru Nanocolumns Induced by Residual Oxygen. *J. Nanosc. Nanotech.* 7(6), 2192–2196. DOI: 10.1166/jnn.2007.793.

21. David, W.I.F., Shankland, K., Mcusker, L.B. & Baerlocher, Ch. (2002). *Structure Determination from Powder Diffraction Data (SDPD)*, Oxford Science Publications, New York, USA.

22. Alghamdi, M.T., Alsibaai, A.A., Shahawi, M.S. & Refat, M.S. (2016). Synthesis and spectroscopic studies of levofloxacin uni-dentate complexes of Ru(II), Pt(IV) and Ir(III): Third generation of quinolone antibiotic drug complexes, *J. Mol. Liq*. 224, 571–579. DOI: 10.1016/j.molliq.2016.10.038.

23. Chen, L., Yuan, C., Gao, B., Chen, S. & Zhang, X. (2009). Microwave-assisted synthesis of organic–inorganic poly(3,4-ethylenedioxythiophene)/$RuO_2{\cdot}xH_2O$ nanocomposite for supercapacitor. *J. Solid-State Electrochem*., 13, 1925–1933. DOI: 10.1007/s10008-008-0777-y.

24. Sugimoto, W., Iwata, H., Murakami, Y. & Takasu, Y. (2004). Electrochemical Capacitor Behavior of Layered Ruthenic Acid Hydrate. *J. Electrochem. Soc*., 151(8), A1181. DOI 10.1149/1.1765681.

25. Alibrahim, K.A., Al-Fawzan, F.F. & Refat, M.S. (2019). Chemical Preparation of Nanostructures of Ni(II), Pd(II), and Ru(III) Oxides by Thermal Decomposition of New Metallic 4-Aminoantipyrine Derivatives. Catalytic Activity of the Oxides. *Russ. J. Gen. Chem*., 89, 2528–2533. DOI: 10.1134/ S1070363219120326.

26. Refat, M.S., Saad, H.A., Gobouri, A.A., Alsawat, M., Belgacem, K., Majrashi, B.M. & Adam, A.M.A. (2021). RuO2 Nanostructures from Ru(III) Complexes As a New Smart Nanomaterials for Using in the Recycling and Sustainable Wastewater Treatment: Synthesis, Characterization, and Catalytic Activity in the Hydrogen Peroxide Decomposition. *Russ. J. Phys. Chem. A*, 95, S346–S351. DOI: 10.1134/ S0036024421150218.